A Novel 3D Optical Proximity Sensor Panel and its Readout Circuit

Tzu-Yang Lin[1], Paul C.-P. Chao[1,2,*], Wei-Dar Chen[1], and Che-Hung Tsai[1]
[1]Department of Electrical Engineering, National Chiao Tung University, Hsinchu 300, Taiwan
[2]Institute of Imaging and Biomedical Photonics, National Chiao Tung University, Tainan 711, Taiwan
*Email: pchao@mail.nctu.edu.tw, TEL: +886-3-5131377, FAX: +886-3-5752469

***Abstract*—This study presents a novel 3D optical proximity sensor (3D OPS) array panel. The panel is capable of detecting the objectives centimeters away from the panel surface. This device is composed of light-emitting diodes and home-made polymer photo-detectors (PPDs). The novel design of the circuit is the operation principle through active pixel circuit, sampling circuit, amplifier circuit and the decision of proposed chip parameters is determined by circuit simulation. The circuit is regarded low power and low cost as the design principle. The control sequence of the aforementioned circuit module is generated by an FPGA board to realize the operation of the whole circuit. The readout circuit is able to remove background current, and to detect the corresponding output voltage of photocurrent that is received by the PPD via reflections of the measured object. A human machine interface is built by LABVIEW to create 3D vision tracing of sensed object, validating the effectiveness of the 3D OPS.**

***Index Terms*—Proximity sensor, photodiode, readout circuit.**

I. Introduction

This study proposes a novel 3D optical proximity sensor (3D OPS) array panel for detecting the three dimensional coordinates of a an object to detect. The optical proximity sensor (OPS) is widely used in new applications in wireless communications, bio-molecular sciences, environmental monitoring [1], and displays [2]. Especially for display applications, the designed 3D OPS panel could be an integral part of a future 3D touch panel. Usually, the sensing component of the pixel is an inorganic polymer photo-detector (PPD), e.g., a-Si photodiode [3], or an inorganic photo-gate (CMOS technology) [4]. By CMOS technology, the PPD is mainly a photodiode. In operations, the light source produces a light signal and then the light signal is received by the PPD via the reflections of the measured object. The PPD next transfers the light signal to the electrical signal [5]-[8]. By detecting the intensity of the electrical signal, the OPS can detect the distance of measured object.

The OPS proposed in this study consists of a light source, like a light emitting diode (LED), and an array of polymer photo-detectors (PPDs) [9]. The LED normally operates in low voltage and emits high brightness. As a result of the band-gap of the organic materials, the organic molecules in PPDs absorb the light in visible spectral range. Therefore, the PPDs are able to detect the photocurrent, which includes the background current and the current which is received by reflections of the measured object.

This study designs a readout circuit that consists of active pixel circuit [10]-[15], sampling circuit and differential amplifier circuit, which are responsible for the OPS to remove background off current and correctly read out the corresponding output voltage of photocurrent that is received by PPD, based on reflections of the measured object.

II. Operation Principles

A. System description

The OPS is composed of an array of LEDs and PPDs. The light emitted by the LEDs is reflected from the measured object and traces back onto the PPD pixels. The architecture of OPS is shown in Fig. 1, where the PPDs and the readout circuit convert the light signal to the electrical signal. By differentiating varied intensities of the electrical signals, the designed readout circuit can generate different output signals that are proportional to the light intensity.

B. Sensing theory

The operation of OPS is presented in this subsection. The relationship between the detected object and the OPS is shown in Figs. 2. The LED is assumed to be a Lambertian emitter and the object a Lambertian reflecting surface [5]. The radiant flux from the LED that is detected by PPD is proportional to $cos\theta \times \Omega$, where Ω is the solid angle spanned by the PPD to the object and it can be obtained by

$$\Omega = \frac{A_{PPD} \cdot \cos\theta}{d^2 + (x - x^*)^2 + (y - y^*)^2}, \quad (1)$$

where d is the distance between the object and the sensor; θ is the angle between the PPD and the object; x and y are the coordinates of the sensing PPDs in x-y plan, respectively; x^* and y^* are the coordinates of the object in x-y plan; and A_{PPD} is the area of the PPD pixel. The photocurrent I output by the PPD is then

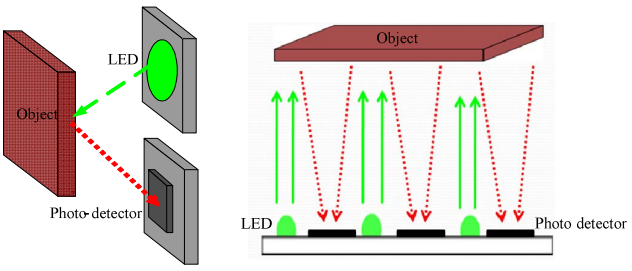

Fig. 1. The architecture of proximity sensor.

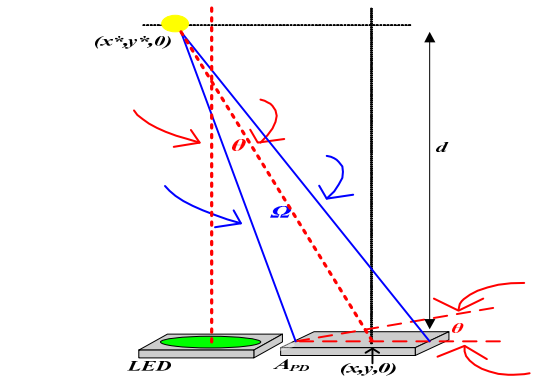

(a)

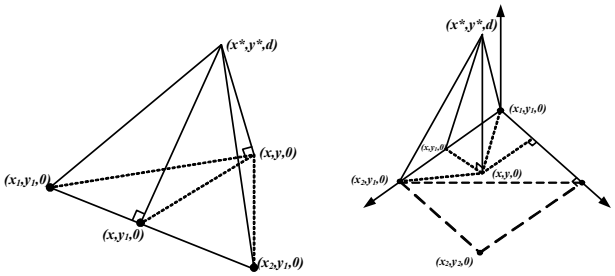

(b)

Fig. 2. (a) Side view of sensor and light source; (b) Relationship of the position of the object and space coordinates.

$$I_i\left(x^*,\ y^*,\ d\right)=\frac{\alpha d^2}{\left[d^2+\left(x_i-x^*\right)^2+\left(y_i-y^*\right)^2\right]^2},\ i=1,\cdots,9, \tag{2}$$

where α is a proportionality factor to be calibrated. The positions of the PPDs are $(x_1, y_1, 0)...(x_9, y_9, 0)$ in 3x3 PPD array. The position of the object to detect is (x^*, y^*, d). When the object approaches a given pixel of the PDD array, nine pixels of PPDs generated photocurrents and give the output voltage of the designed pixel circuit as

$$V_{out,\,i}=\frac{A_d T_t}{C_{in}}\left(I_i\right),\ \ i=1,\cdots,9, \tag{3}$$

where $V_{out,\,i}$ is the output voltage; A_d is the differential gain; T_t is the integration time and C_{in} represents the photodiode capacitor in parallel with the equivalent capacitance C_{MOS} of MOS transistors seen at node a and a storage capacitor C_s in Fig. 5(b). Incorporating Eq. (3) into (2), the pixel output voltage due to the photocurrent is then

$$V_{out,\,i}=\frac{\beta d^2}{\left[d^2+\left(x_i-x^*\right)^2+\left(y_i-y^*\right)^2\right]^2},\quad i=1,\cdots,9, \tag{4}$$

where

$$\beta=\frac{\alpha A_d T_t}{C_{in}}. \tag{5}$$

To figure out the 3D coordinates of the sensed object based on Eq. (4), three different voltage outputs based on Eq. (4) from three different PPDs have been available for solving three different equations in the form of Eq. (4). It is determined when a object is to be sensed that three PPDs with maximum voltage outputs are considered to calculate the 3D coordinates of the the object based on

$$V_{out,\,\text{largest}}=\frac{\beta d^2}{\left[d^2+\left(x_1-x^*\right)^2+\left(y_1-y^*\right)^2\right]^2}, \tag{6}$$

$$V_{out,\,\text{second}}=\frac{\beta d^2}{\left[d^2+\left(x_2-x^*\right)^2+\left(y_2-y^*\right)^2\right]^2}, \tag{7}$$

$$V_{out,\,\text{third}}=\frac{\beta d^2}{\left[d^2+\left(x_3-x^*\right)^2+\left(y_3-y^*\right)^2\right]^2}. \tag{8}$$

A nonlinear equations-solver by MATLAB is forged herein to solve Eqs. (6-8) for the coordinates of the object, (x^*, y^*, d).

III. Fabrication Process

A. Photodiodes (PDs)

The fabrication process of the PPD array fabrication is illustrated by Fig. 3, which is divided into the following steps. First, polymer photodiode pixels are fabricated by patterning

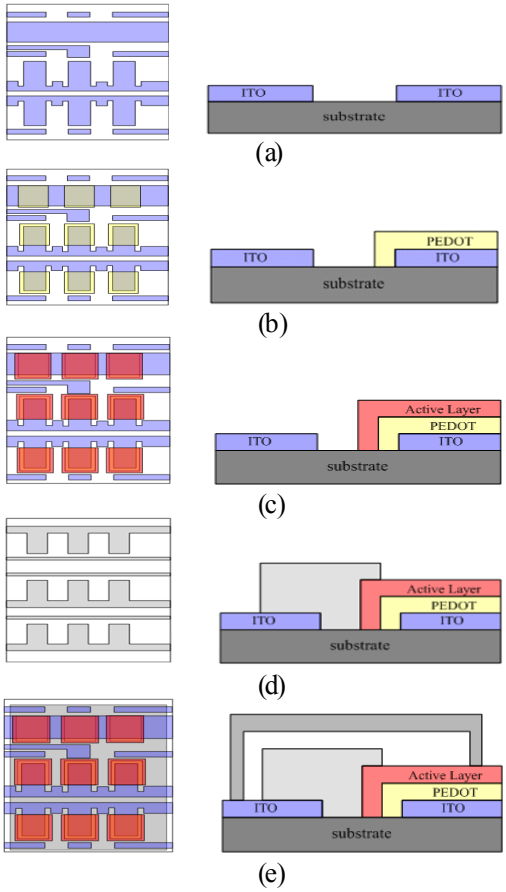

Fig. 3. Top view and cross section of (a) ITO pattern; (b) deposition of the PEDOT:PSS; (c) deposition of the active polymer layers; (d) evaporate metal electrode; (e) the 3x3 PPD array.

the indium tin oxide (ITO) layer with a thickness of 180 nm as shown in Fig. 3(a). In the second step, a 50 nm thick layer of poly-(3,4-ethylenedioxythiophene): poly-(styrenesulfonate) (PEDOT: PSS) is applied by spin-coating on the patterned ITO substrate. PEDOT: PSS, as shown in Fig. 3(b), is the hole-input horizon layer in PD and has an advantage to prevent short circuit effectively. An active layer of poly (3-hexylthiophene) (P3HT) and a (6,6)-phenyl-C_{61}-butyric acid methyl ester (PCBM) is next spin-coated a on the PEDOT: PSS layer, where P3HT is the donor and PCBM the acceptor, as shown in Fig. 3(c). A 350 nm thick layer of calcium capped by 1000 nm of aluminum is deposited as cathode layer (Fig. 3(d)). Finally, there are three remaining steps to encapsulate devices. First, the encapsulated glass is formed to the glove box. Second, packaging resin is used to smear over the encapsulated glass, and a hygroscopic agent is used to paste the encapsulated glass. Then, the encapsulated glass is pressed on the evaporated device. Finally, it is exposed with ultraviolet (UV) for five minutes and perform encapsulation. A top view of the 3x3 PPD array is shown in Fig. 3(e).

B. Performance measurements

The incident photon-to-current conversion efficiency (IPCE) is main performance index of a PPD which can be defined by

$$IPCE(\%) = \frac{1240(eV \cdot nm) \times photocurrentdensity(A/cm^2)}{wavelength(nm) \times powerdensity(W/cm^2)} \quad (9)$$

To measure IPCE of the PPDs, the light source with a 250W quartz-tungsten-halogen lamp and monochromator is selected single-wavelength light, and then the photocurrent generated by PPD is measured. The measurement results of the IPCE is shown in Fig. 4, where the measured IPCE is seen close to the absolute spectrum, giving a maximized PD performance.

IV. READOUT CIRCUIT AND SYSTEM

A. PPD pixel circuit

In this study, the two transistors active pixel circuits (2T-APC) which can substitute for the three transistors (3T), as shown in Fig. 5(a), to apply to the proximity sensor array is proposed. The simplified 2T circuit can provide improvement in electrical performance. For low cost, the polymer photodiode is used to replace the organic one in the light-sensitive component of the pixel. The novel pixel circuit consists of a PPD, a reset transistor (*M1*), a row select transistor (*M2*) and a storage capacitor. *M1*and *M2* adopts PMOS structure. Fig. 5(b) shows the schematic of 2T-APC. The 2T-APC operates in three modes:

(i) Reset: The reset transistor (*M1*) and row select transistor (*M2*) are switched ON and pre-charges the node V_a and C_s to 3.3V.

(ii) Integration: After reset, *M1* is switched OFF for an integration period (T_t). During T_t, the photodiode voltage (V_a) drops, since the photo-carriers discharge C_s and C_{PD}.

(iii) Readout: After integration, *M2* is switched OFF and read out the V_{out}. Because the *M2* acts as ideal switch (V_{DS2}=0), V_a is equal to V_{out}. At the end of integration, the output voltage of *M2* can be expressed as

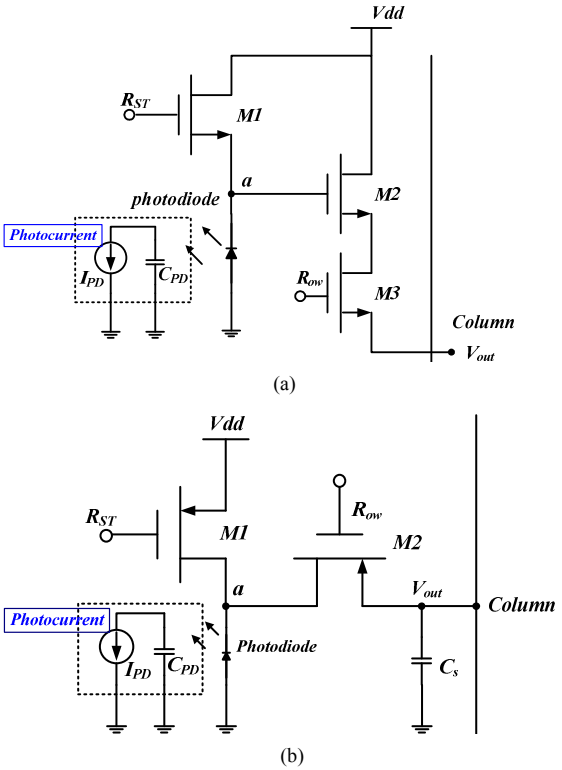

Fig. 5. (a) The schematic of a 3T-active pixel circuit; (b) a 2T-active pixel circuit.

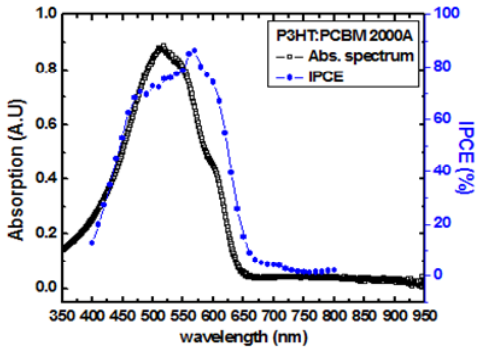

Fig. 4. The incident photon-to-current conversion efficiency.

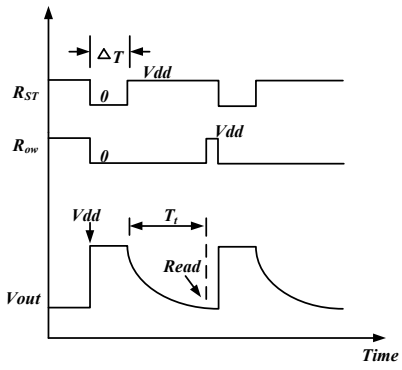

Fig. 6. Timing diagram of 2T-active pixel circuit.

$$V_{out} = V_{dd} - \frac{T_t}{C_{in}} I_{PD}, \tag{10}$$

where T_t is the integration time while capacitance C_{in} represents the photodiode capacitor in parallel with the equivalent capacitance C_{MOS} of MOS transistors seen at node a and storage capacitor C_s; thus,

$$C_{in} = C_{PD} + C_{gd1} + C_{gd2} + C_s. \tag{11}$$

The associated timing diagram of 2T-APC is shown in Fig. 6.

B. Readout circuit

A schematic of the readout circuit is shown in Fig. 7. The readout circuit, which is common to an entire column of pixels, includes two sampling circuits for storing the signal levels. Each sampling circuit consists of a sampling transistor (*M3* or *M4)* and a capacitor (C_{SHR} or C_{SHR1}). The timing diagram for the readout circuit is shown in Fig. 8. Firstly, the LED is switched OFF in the first reset cycle. Then, the reset transistor (*M1*) is switched ON and pre-charges V_a to 3.3V. At the same time, the row select transistor (*M2*) is switched ON. After reset, *M1* is switched OFF for an integration period (*t=t1*). During *t1*, PD generates the photo-carriers discharging C_{PD} since ΔQ decreases V_a. Before *M2* is switched OFF, V_1 is sampled onto capacitor C_{SHR} by pulsing *M3* to V_{DD}. Let V_1 reflects the background voltage. Secondly, the LED is switched ON in the

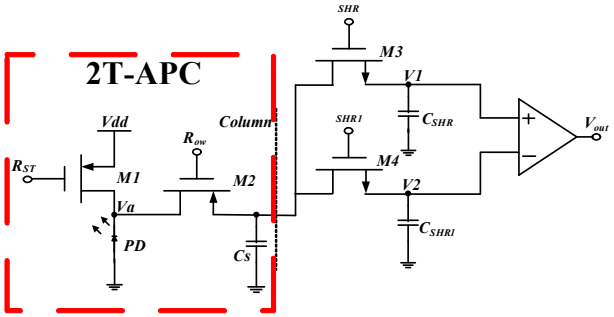

Fig. 7. The schematic of the readout circuit.

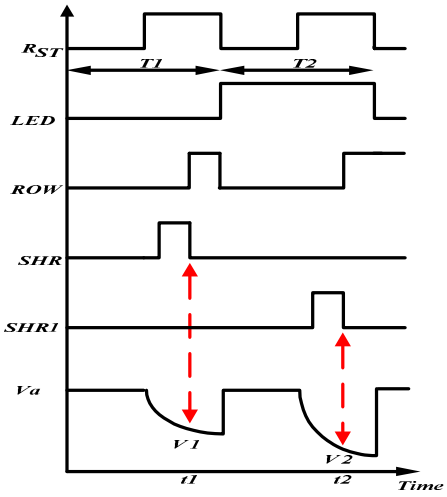

Fig. 8. Timing diagram for readout circuit.

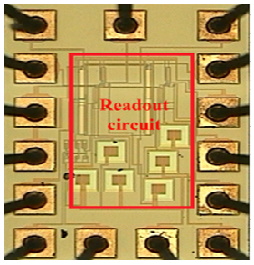

Fig. 9. The micrograph of the IC.

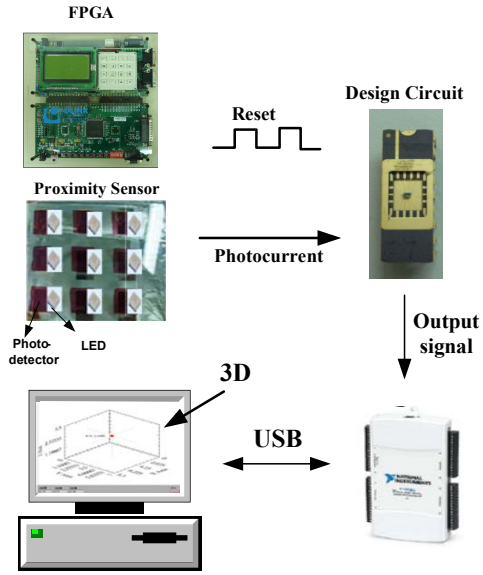

Fig. 10. System architecture of the testing environment.

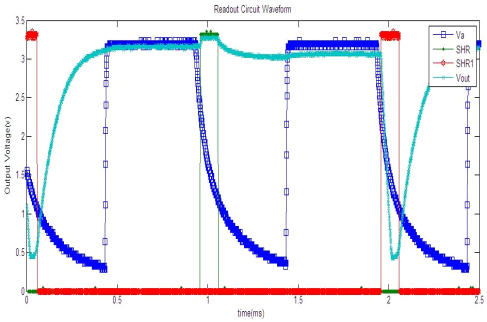

(a)

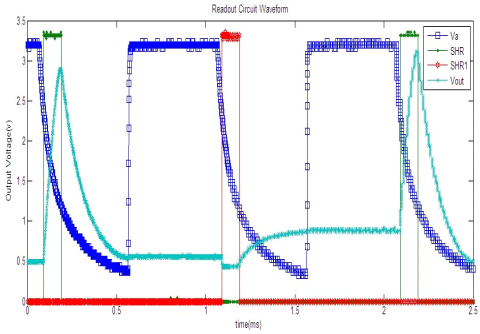

(b)

Fig. 11. (a) Measurement of the output signal at 1.5cm distance; (b) at 2.9cm. distance.

second reset cycle. Then, the reset transistor (*M1*) is switched ON and pre-charges V_a to 3.3V At the same time, the row select transistor (*M2*) is switched ON. After reset, *M1* is switched OFF for an integration period (*t=t2*). During *t2*, PD generates photo-carriers discharging C_{PD}, and ΔQ decreases V_a. Before *M2* is switched OFF, V_2 is sampled onto capacitor C_{SHR1} by pulsing *M4* to V_{DD}. Moreover, V_2 represents the background voltage and the voltage of reflected light. Then the differential amplifiers subtracts V_2 from V_1 to obtain the voltage proportional to the reflected light. V_{out} can be expressed as

$$V_{out}(T_2) = A_d(V_2 - V_1), \tag{12}$$

where T_2 is the period for the LED switched OFF and A_d is the differential gain. The micrograph of the IC is shown in Fig. 9.

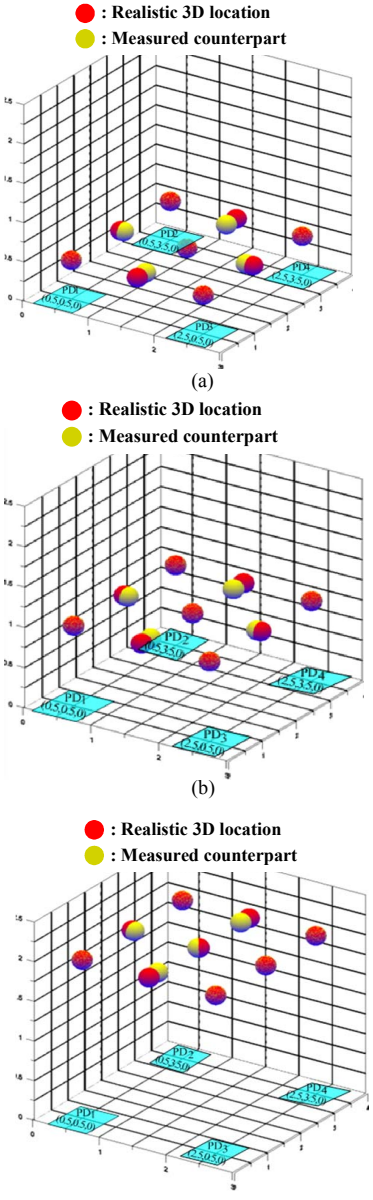

Fig. 12. The 3D coordinates at (a) 0.5cm; (b) 1cm; (c) 2cm distance.

C. *Experimental results*

The system description of the testing environment is shown in Fig. 10. The control signals of Rst, Row, SHR, SHR1, LED in Fig. 8 are generated by FPGA to confirm the designed integrate circuit. The output signal of integrated circuit is captured by data acquisition (DAQ) to computer. The algorithm is established into the computer database by LABVIEW for the 3D vision tracing. Comparison is performed between the measuring coordinates and the setting realistic coordinates in 3D. At last, Figs. 11(a) and (b) present experimental results that are the measurement of the output signal at 1.5cm and 2.9 cm distance. For 3D vision tracing, the intensive light emitted by LED is used with the OPS for real-time image generation. An human finger, as small as 1.2 cm in diameter, is tested for mini-scale 3D image generation experiment integrated with the home-made PPD and LED with its integrated circuit. A 2x2 array is utilized to verify the accuracy of the established equation. The 3D coordinates of measured object is captured by LABVIEW system, which measure the object with the heights of 0.5cm, 1cm and 2cm. Comparison between the measuring and the realistic coordinates in 3D is shown in Fig. 12, where the red balls represent the realistic coordinates, and the yellow ones are the predicted coordinates. These experimental results generally show that the sensing theory with the designed readout circuit can detect the 3D coordinate efficiently.

V. Conclusion

In this paper, a novel 3D optical proximity sensor is proposed and its readout circuit can deal with the background off current and the unwanted light from the surrounding. This paper also proposes 3D optical proximity sensor to realize real-time detection of the sensed objects in the X, Y, Z directions. A human machine interface is constructed by LABVIEW to create 3D vision tracing. Moreover, the LED plays an important role in 3D proximity technology, since the direction of reflection has an impact on detecting position.

Acknowledgment

The authors are greatly indebted to National Chip Implementation Center and National Science council of R.O.C. for the supporting research through contacts in nos. NSC 98-2622-E-009-006-CC1.

References

[1] D. Um and Wayne N.P. Hung, "A Novel Infrared Proximity Array Sensor for 3D Visual Sensing: Modeling and Applications," IEEE International Conference on Robotics and Automation, 2006.

[2] T. Vaithianathan, Iain D. C. Tullis, N. Everdell,T. Leung, A. Gibson, J. Meek and D. T. Delpy, "Design of a portable near infrared system for topographic imaging of the brain in babies," American Institute of Physics, vol. 75, no. 10, pp. 3276-3283, 2004.

[3] M. Maolinbay, Y. El-Mohri, L. E. Antonuk, K.- W. Jee, S. Nassif, X. Rong, and Q. Zhao, "Additive noise properties of active matrix flat panel imagers," Med. Phys., vol. 27, no. 8, pp. 1841–1854, Aug. 2000.

[4] S. K. Mendis, S. E. Kemeny, and E. R. Fossum, "CMOS active pixel image sensor," IEEE Trans. Electron Devices, vol. 41, no. 3, pp. 452–453, Mar. 1994.

[5] T. Fukuda, "Optical Semiconductor Device", John Wiley & Sons, 1999.

[6] A. Neamen, “Semiconductor Physics & Devices”, McGraw- Hill, 1999.
[7] D. Cristia, P. Cosmin, and F. Craciunoiu, “High-Responsivity Silicon Photodetectors for Optoelectronic Integrated Systems,” Proceedings of the International Semiconductor Conference, CAS, vol. 1, pp. 215-218, 1996.
[8] L. Simpson, M. Nance Ericson, Gerald E. Jellison, William B. Dress, Alan L. Wintenberg, and M. Bobrek, “Application Specific Spectral Response with CMOS Compatible Photodiodes,” IEEE Transactions on Electron Devices, vol 46, n 5, pp. 905-913, 1999.
[9] E. Chen, S. Tseng, J. Ju,1 C. Yang, H. Meng, S. Horng, and C. Shu, “ Polymer infrared proximity sensor,” Applied Physics Letters, vol 93, n 6, 2008.
[10] R. Street, “Large area image sensor array,” in Technology and Applications
of Amorphous Silicon, R. A. Street, Ed. Berlin, Germany: Springer-Verlag, ch. 4, pp. 147–221, 2000.
[11] K. S. Karim and A. Nathan, “Readout circuit in active pixel sensors in amorphous silicon technology,” IEEE Electron Device Lett., vol. 22, no. 10, pp. 469–471, Oct. 2001.
[12] K. S. Karim, A. Nathan, and J. A. Rowlands, “Amorphous silicon active pixel sensor readout circuit for digital imaging,” IEEE Trans. Electron Devices, vol. 50, no. 1, pp. 200–208, Jan. 2003.
[13] K. S. Karim, A. Nathan, J. A. Rowlands, and S. O. Kasap, “X-ray detector with on-pixel amplification for large area diagnostic medical imaging,” Proc. Inst. Electr. Eng.—Circuits Devices Syst., vol. 150, no. 4, pp. 267–273. Aug. 2003.
[14] L. Jackson, N. Arokia and R. John, “ High dynamic range active pixel sensor arrays for digital x-ray imaging using a-Si:H,” Journal of Vacuum Science and Technology A: Vacuum, Surfaces and Films, vol 24, n 3, pp.850-853, 2006.
[15] F. Dadouche a, A. Pinna a, P. Garda a, and A. Alexandre-Gauthier , “ Modelling of pixel sensors for image systems with VHDL-AMS,” International Journal of Electronics, vol 95, n 3, pp. 211-225, Jan. 2008.